Available online at www.sciencedirect.com

Manufacturing Letters

Manufacturing Letters 41 (2024) 850–861

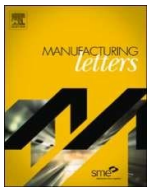

52nd SME North American Manufacturing Research Conference (NAMRC 52, 2024)

Machine tool cross beam design, fabrication, and testing using metal big area additive manufacturing

Tyler Poon[a], Justin L. West[a,b], Emma D. Betters[a,b], Scott Smith[b], Christopher T. Tyler[b], Andrzej Nycz[b], Christopher Masuo[b], and Tony Schmitz[a,b]*

[a]Univeristy of Tennessee, Knoxville, 1512 Middle Drive, Knoxville, TN 37996, USA
[b]Oak Ridge National Laboratory, Manufacturing Demonstration Facility, 2350 Cherahala Bld., Knoxville, TN 37932, USA

* Corresponding author. Tel.: +1-865-974-6141. E-mail address: tony.schmitz@utk.edu.

Abstract

This paper describes the application of metal Big Area Additive Manufacturing (mBAAM) to the fabrication of a machine tool cross beam. The replacement of a traditional box design weldment with a new design printed by wire arc additive manufacturing using the MedUSA system at Oak Ridge National Laboratory (ORNL) is detailed. This requires a new design strategy based on the unique mBAAM capabilities. The intent of the new design is to reduce mass, while maintaining the dynamic stiffness. To compare the two designs, the natural frequencies and mode shapes are measured using impact testing and predicted using finite element analysis. It is confirmed that the printed structure dynamics agreed with the numerical model predictions, which demonstrates that it is feasible to model a large-scale mBAAM part and understand its behavior prior to printing. Another notable outcome of this study is that the significant residual stress and distortion in the print indicate that knowledge gaps remain for widespread implementation of mBAAM.

Peer-review under responsibility of the Scientific Committee of the NAMRI/SME.
Keywords: Additive manufacturing; finite element analysis; machine tool; modal analysis

1. Introduction

This paper describes the design of a machine tool cross beam using metal big area additive manufacturing (mBAAM). The cross beam is part of a concrete base machine tool [1] designed and produced at Oak Ridge National Laboratory (ORNL); see Figure 1. A steel box tube weldment serves as the cross beam for the machine tool. For this project, mBAAM was selected to design and fabricate a new cross beam to serve as a replacement for the current weldment. This required a new design strategy based on the unique mBAAM capabilities. It was desired to reduce mass in the new design, while maintaining the dynamic stiffness. The ORNL MedUSA system provided the wire arc additive manufacturing (WAAM) deposition capabilities for this project [2].

The mBAAM process is a subset of big area additive manufacturing (BAAM) [3], which increases the scale of AM by choosing feasible technologies for scale up including higher deposition rates. mBAAM leverages WAAM and laser wire additive manufacturing (LWAM) [3], which offer higher metal deposition rates compared to other printing techniques. Some challenges associated with WAAM are thermal

distortions, interlayer strength, and post processing requirements.

To provide a basis for the new design, the weldment cross beam was modeled using finite element analysis (FEA). The predicted static and dynamic deflection behavior served as design inputs for the WAAM cross beam. To validate the FEA model, modal analysis was completed using impact testing on the cross beam weldment. To avoid the influence of boundary conditions, a replica of the cross beam was produced and all testing was completed in a free-free state (i.e., suspended from flexible straps). Natural frequencies and mode shapes were measured and compared to the FEA predictions.

The WAAM cross beam included several design constraints. Because the cross beam must be mounted to an existing machine tool, the connections needed to match the twin column geometry shown as the left and right vertical columns in Figure 1. Additionally, the design had to incorporate the capabilities and limitations of the MedUSA system, which uses three robotic arms to simultaneously deposit material using WAAM. Example considerations include robot conflicting workspace and reachability. Various concepts were generated and eliminated through FEA models and design reviews. A final design was selected that met the following criteria: 1) comparable stiffness to the current weldment; 2) lower mass than the current weldment; and 3) could be printed using MedUSA using an appropriate combination of the three robots. The final design was printed on the MedUSA system. However, the deposition was stopped prior to completing the cross beam design due to significant thermal distortion. The remainder of the paper is organized as follows. Section 2 describes the weldment design and evaluation using FEA and measurements. Section 3 describes the WAAM cross beam design and evaluation. Section 4 details the FEA modeling, Section 5 provides the fabrication information, and Section 6 gives experimental results.

The cross beam print revealed mBAAM technology challenges. The part deformation caused the print to be discontinued. Although the print was not completed, the implementation of the design, manufacturing, and testing processes provides a methodology for future mBAAM projects.

2. Weldment cross beam design

2.1. Concrete base machine

The cross beam weldment was designed for the concrete base machine at ORNL. The three-axis, vertical spindle concrete base machine tool was intended to demonstrate the capability to address supply chain challenges for the large metal castings typically selected as machine tool bases [1]. The cross beam is mounted on top of the concrete base vertical columns and the spindle and Z-axis assembly are attached to the weldment identified in Figure 1.

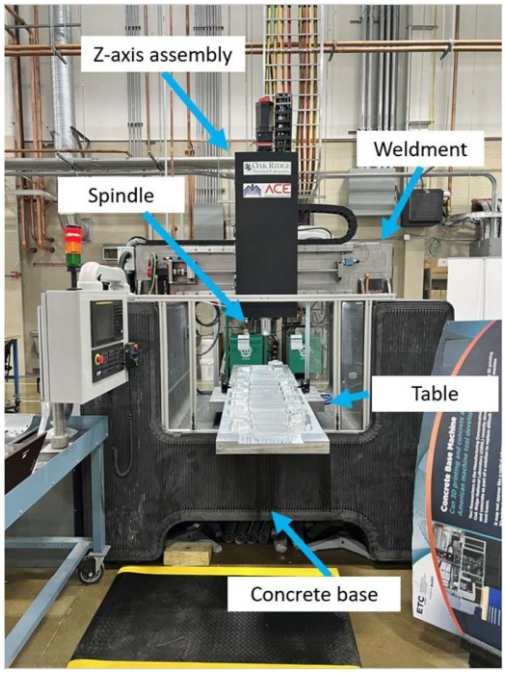

Fig. 1. Concrete base machine tool with the cross beam weldment supporting the Z-axis and spindle assembly.

The cross beam, shown in Figure 2, connects the base and the Z-axis assembly. The cross beam is mounted onto the concrete base through bolts to metal plates on each side of the machine tool. The metal pads were leveled to ensure that the cross beam would sit flat on top of the machine tool base and be mounted securely. The front face of the cross beam is where the guide rails and motors for the Y-axis motion are mounted. The Z-axis assembly, which carries the spindle, is connected to the guideways through bearing pads. In addition to supporting the spindle and Z-axis (or column assembly), the cross beam was used for mounting cables and tubing for the machine operation.

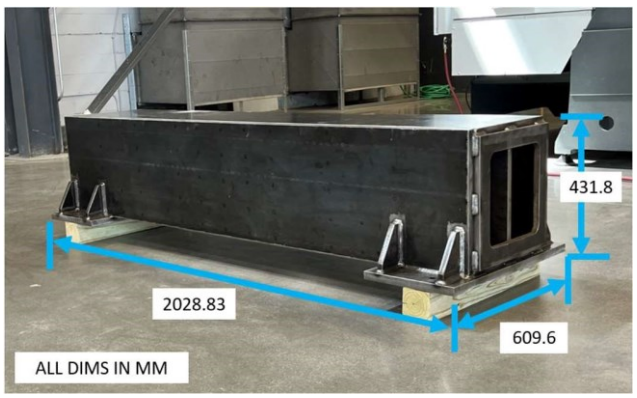

Fig. 2. Cross beam weldment.

The cross beam weldment was an assembly of welded steel plates. It was comprised of one main rectangular box section that has an internal supporting rib and two footpads that support each end of the box. The weldment construction included an Lshaped weldment because the bottom and front plates were necessary for mounting the column assembly as well as the mounting feet to the base. The top, back, and side plates were added to form a box tube geometry. After static analysis, an internal rib was added to stiffen the box since the mass of the column assembly is cantilevered from the front face. A critical design feature of the weldment was that the front face is the primary mounting surface for the Y-axis guide rails and motor assembly. The second key mating surfaces were the two steel feet that mount to the concrete base. The final design shown in Figure 2 provided the required mounting surfaces and enabled the box structure to support the column assembly.

2.2. Weldment details

The cross beam weldment dimensions were 2029 mm by 610 mm by 432 mm. The individual A36 steel plates were welded together to create the final structure.

The cross beam weldment was outsourced for manufacturing; this weldment for this project was identical to the original design for the concrete base machine tool, but was available for free-free boundary condition impact testing and comparison to the FEA predictions and mBAAM cross beam. Because the plates needed to be welded, chamfers were added to the edges of the selected plates.

3. mBAAM cross beam design

3.1. MedUSA description

The ORNL MedUSA system [2] shown in Figure 3 was used to print the cross beam. The MedUSA system was created for mBAAM and was designed to print WAAM parts. The intent of the cross beam redesign was to ensure comparable static and dynamic behavior of the structure and reduce mass relative to the weldment, while also making it compatible with the WAAM process and the MedUSA system.

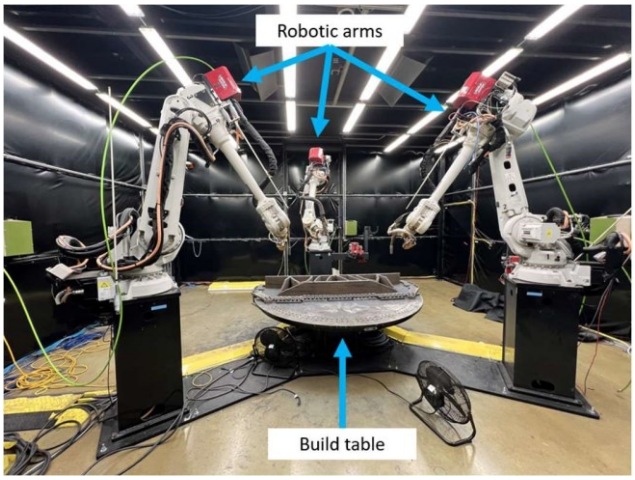

Fig. 3. MedUSA system at ORNL used to print the WAAM cross beam.

The cross beam redesign was provided as a case study to establish the feasibility of making a WAAM part to match or exceed the performance of a traditional weldment and learn more about the capabilities of the MedUSA system. MedUSA has previously been used to create complicated demonstration parts that challenge the system's capabilities. The limitations and capabilities of MedUSA are constantly evolving and the design of the WAAM structure was therefore completed in collaboration with the ORNL experts that operate the system.

3.2. Design approach

The design process for the WAAM cross beam was iterative. Many designs were conceptualized and analyzed. With each iteration, the design was refined to meet the project goals. The WAAM cross beam was designed to replace the weldment cross beam with the intent of reducing the mass of the structure, while retaining the weldment's stiffness.

Critical surfaces and clearance profiles needed to be maintained between the weldment and WAAM structure. For the WAAM print to mate with the concrete base as well as the column assembly, the mounting feet and rail locations were preserved. For the mounting feet, the plate sizes, hole sizes, and plate locations were kept constant. The front face of the WAAM cross beam was designed to have the same guide rail locations and clearance profile as the weldment. Maintaining both the mounting feet and front face mounting profiles provided a direct method for comparing the various WAAM designs to the weldment's deflection under load.

During the design iterations, various cross-sections and mass reduction patterns were implemented. To avoid overhangs, two-dimensional patterns were extruded to generate wall features for the WAAM cross beam. The design was required to be fully produced using WAAM. For example, adding external plates (by welding) to the structure to improve stiffness was not allowed. Concepts with mass that exceeded the weldment (702 kg) were also excluded.

FEA models were used to compare designs. Comparison of each design's deflections to the weldment deflections was used to assess the new design's feasibility. As noted, mass was also used as a selection metric. Finally, the design selection

was based on feedback from the ORNL WAAM team. The WAAM team assessed the printing feasibility for each design that met the mass and stiffness requirements. In addition, the team made design suggestions that would enable preferred print strategies to be implemented. Integrating the manufacturing team's input into the design process reduced the need for major modifications later in the project.

Important design factors are summarized:

- There is a list of materials that are compatible with the MedUSA cell; LA100 from Lincoln Electric was selected for its weldability and strength.
- Material properties can differ from the wire properties and can be position-dependent due to the WAAM process heating and cooling profiles and temperature gradients.
- The print bead width can vary from 6 mm to 8 mm.
- The print must be made on a build plate (or several build plates).
- The WAAM process has shown better results for continuous bead prints than short, segmented print paths due to reduction in traveling moves caused by maintenance routines (i.e., trimming the welding wire) after the end of a toolpath.
- Weld beads that cross one another should be minimized to avoid overgrowth that can cause torch-to-part collision and, if necessary, there should be only one bead intersection.
- The design must be able to be sliced using the ORNL slicing software, which generates the robots' tool paths.
- The printed surface will be wavy (up to 1.5 mm surface height variation) and the cross-sectional area that is used for calculating mechanical properties must account for the surface variations.
- The WAAM process is not suitable for printing large flat surfaces or walls due to thermal deformations and print time and cost.
- Overhangs should generally be avoided, but 20° to 25° angles from vertical are possible.
- If there is a surface that needs to be finished (by machining, for example), there should be at least 3 mm of additional material.
- Features should be at least two beads thick and there should be adjacent bead overlap (slicer limitation).

3.3. Final design

After reviewing the FEA simulation results, a final WAAM design, shown in Figure 4, was selected. The overall dimensions are 2028.8 mm by 609.6 mm by 601.4 mm.

A feature of the final WAAM design is catenary arches on the front and back faces. Catenary arches have been implemented in many structures, such as buildings or bridges. Catenary arches are described using the hyperbolic cosine function shown in Equation 1, where a defines the position of the curve apex [4]. This geometry was chosen because it improved the stiffness in the X-Z plane.

$$Z(Y) = a\cosh \quad (1)$$

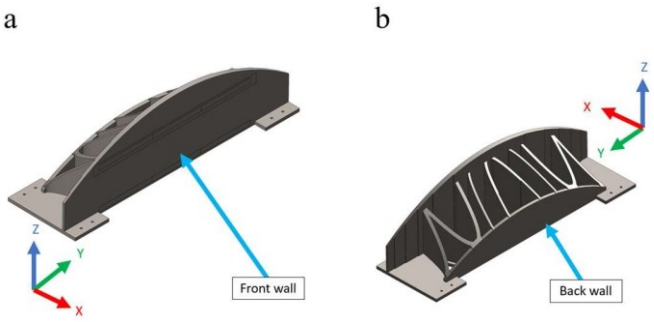

Fig. 4. (a) Front isometric view; (b) back isometric view of the WAAM design

As seen in Figure 4, curved vertical supports connect the front and back walls. These supports increase stiffness significantly while adding little mass. The geometry of the curved supports mimics a sinusoid. The sinusoid provides continuous print paths without sacrificing stiffness. The curved geometry also reduces the number of intersecting beams compared to a honeycomb infill.

The supports are slanted from the front wall to the back to reduce mass while obtaining the required stiffness. The front wall is also thicker in the middle and tapers at the ends. Both features were implemented to add material to the WAAM cross beam where the largest deflections were observed. The additional material improved its stiffness, while minimizing the mass increase.

The build plate for the WAAM deposition was designed to serve as the cross beam base plate. The build plate was separated into five sections of 25.4 mm thick A36 steel plates. By sectioning the base plate into five smaller plates, the build plate was less expensive and easier to purchase. The base plate sizes were selected to provide a clamping border around the base which would later be removed. After deposition, the joints between the individual plates would be welded.

4. Finite element analysis

4.1. Modeling

The cross beam weldment modeling was completed using SolidWorks. Two models were used to investigate the weldment. Both models were simplified from the actual model by removing unnecessary mounting features for the guideways that would have been used for the column assembly. One model is referred to as the simplified model, while the other is referred to as the refined model. The simple model was generated to investigate the static behavior of the system. The refined model was used for the frequency analysis that yielded the natural frequencies and mode shapes of the structure.

The simplified model, shown in Figure 5, included minor modifications to reduce computational complexity. In this model, the welded joints were assumed to be in direct contact and no weld beam geometries were included. The simplified model therefore exhibits stiffer behaviors due to the increase in contact between the modeled surfaces. Each plate and

component were assembled through surface mates. The plates were also assigned material properties of A36 steel.

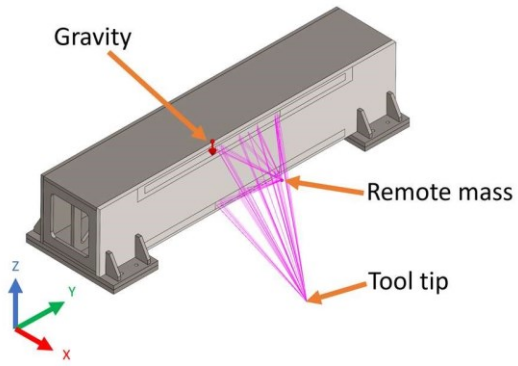

Fig. 5. Simplified model of weldment with remote force locations.

For the static simulations of the simplified weldment, it was important to model the load bearing areas on the front face of the weldment. The simulation was dependent on the model details, and it was necessary to model the area in which the column's load interacts with the guide rails. The load bearing area was calculated using the span of the linear bearing pads that hold the column assembly to both the top and bottom rails. Two configurations were used to investigate the structure's static deflection at its most extreme cases based on the column assembly location. In all cases, the model was supported by the plates located at the bottom of the weldment at each. These plates were assumed to be fixed.

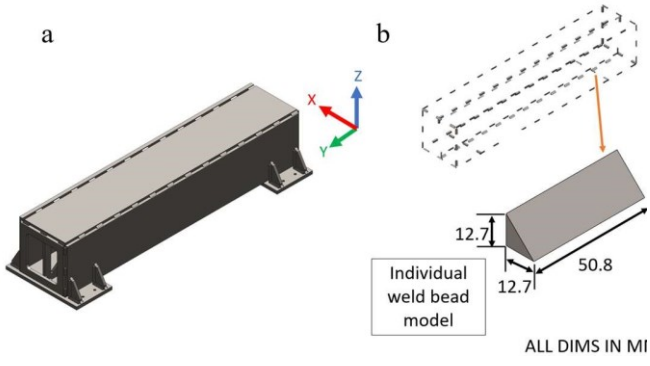

Fig. 6. (a) Refined weldment model; (b) weld bead locations as well as an individual weld bead model

For the refined model, shown in Figure 6, the weld beads were modeled. The refined model was implemented to improve simulation accuracy. The weld beads shown in Figure 6a were modeled by extruding triangular profiles that were attached using the bead patterns specified for the weldment. Per the original drawing requirements, the beads were to have 12.7 mm legs that were 50.8 mm long with a separation of 152.4 mm between each weld bead. Figure 6b shows the weld beam locations and the bead geometry, where material penetration, thermal defects, and bead surface roughness were not considered.

4.2. Mass comparison

The mass of the refined weldment model was used as a baseline. The goal of the WAAM cross beam was to reduce the mass of the structure while maintaining the original stiffness. The weldment material properties were specific using A36 steel values. For the WAAM cross beam, the mass was estimated by assuming no porosity and an average wall thickness based on the overlapping beams.

4.3. Natural frequencies and mode shapes

The structure's dynamic behavior was also predicted using FEA. The frequency simulation from SolidWorks was implemented to predict the natural frequencies and mode shapes, where the refined model, shown in Figure 6, was used for the simulation. Because the welded beads did not entirely seal the edges of the box structure along with its mounting feet, the individual welds needed to be modeled to provide accurate results.

Unlike the static analysis, the frequency analysis of the refined weldment was completed using free-free boundary conditions. To avoid uncertainties introduced by more complicated boundary conditions, free-free conditions were selected because the cross beam could be supported using thin flexible straps to reasonably approximate the simulated freefree ideal.

The material was assigned to be A36 steel in the refined simulation. The plates were modeled per the drawings in addition to the proper assembly and weld bead locations. There were no connections between the plates in the model, and they were assigned free contact behaviors. To provide the motion constraint, all the weld bead contact faces were assigned to bonded conditions to simulate the actual weld. As a result, the refined structure was only held together through the bonded weld beads, which is identical to the physical structure.

Free-free simulation reduced the simulation complexity. No fixtures with assumed connections were required. In addition, no external loads were imposed. A mesh convergence method was implemented to ensure that the results were accurate. With the same initial start mesh size as the simplified model, a mesh element size of 240 mm maximum and 12 mm minimum was chosen for the initial mesh. This was then refined using the variation in the natural frequency of the first dynamic mode with element size reduction. A convergence criterion of less than 5% difference was achieved with a maximum and minimum element size of 15 mm and 0.75 mm, respectively. The remaining parameters were the same as the static simulation.

Due to the structure's mass and size, the dynamic modes occur at relatively low frequencies. The frequency analysis was set to find the modes of the refined weldment from 0 to 5000 Hz. A total of 39 mode shapes were identified in this frequency range, where the first six mode shapes were rigid body modes (i.e., rigid motion of the structure without deformation), which represent its six free-free degrees of freedom.

The first dynamic mode is shown in Figures 7 and 8. It occurred at a frequency of 210 Hz. To enable visual interpretation, the figure's deformation shape is exaggerated. This was done for four other modes relevant to the cross beam performance. The five modes were selected by analyzing the frequency response function (FRF) of the structure and picking the five most dominant modes.

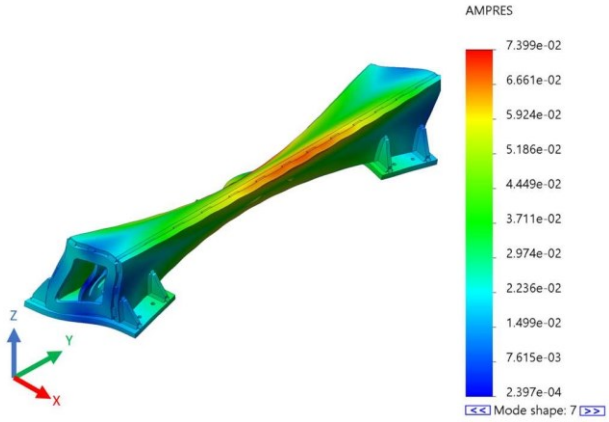

Fig. 7. Mode shape 1 of refined weldment at one extreme deflection state. (The colorbar indicates relative amplitude of motion.)

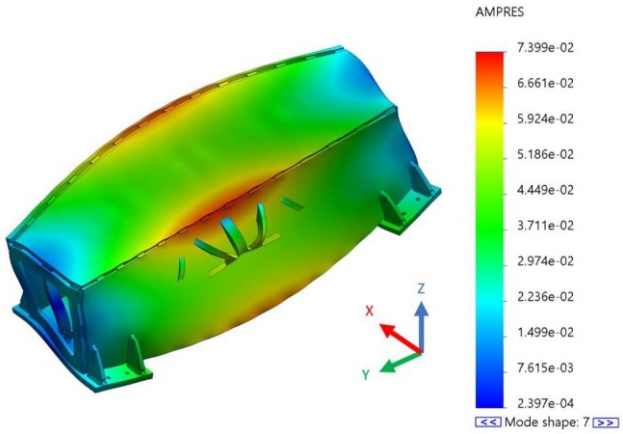

Fig. 8. Mode shape 1 of refined weldment at the other extreme deflection state.

4.4. Modal stiffness

$$k = \qquad (3)$$

Modal fitting of measured FRFs was used to find the damping ratio and stiffness values of the five mode shapes of the bottom and front faces of the weldment and WAAM cross beam. The real and imaginary plots of the impact location

5. Fabrication

5.1. Slicing and path planning

The ORNL WAAM team assisted with the WAAM design. This included input for wall thickness and geometric features that enabled the part to be sectioned for printing using the ORNL slicer. Path planning was completed using an ORNL path planner developed to leverage the three robotic arms and gas metal arc welding torches for the MedUSA system. After

FRFs were used to extract the modal parameters of each system. The modal damping ratio was calculated using Equation 2 and modal stiffness was calculated using Equation 3 for each selected mode [5], where ω_n is the natural frequency, ω_2 and ω_3 are the frequencies for the local maximum and minimum of the real part of the measured FRF, and A is the height of the imaginary peak.

$$\zeta = \frac{-1}{2\omega_n} \qquad (2)$$

the longest print that was attempted on MedUSA, the WAAM team developed end clamps made from 25.4 mm thick A36 steel. Four end clamps were used to secure the four corners of the print.

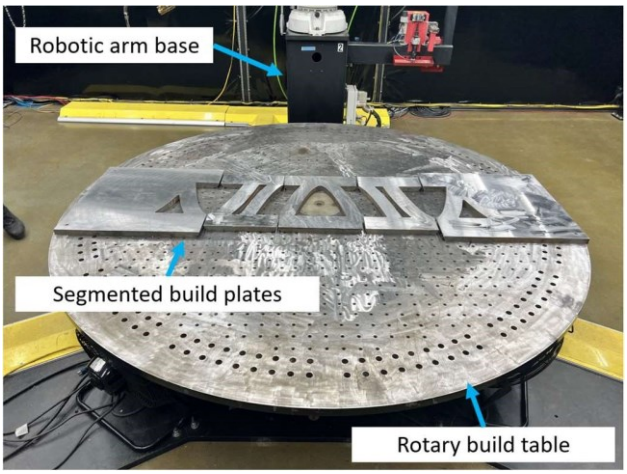

Fig. 9. Segmented build plates on the rotary build table of the MedUSA system. One robotic arm based is shown. Two more are not visible, spaced equally around the build table perimeter.

With the secured build plate, the three robotic arms began printing the WAAM cross beam. The initial layers of the print were the slowest printed layers. The slower print speed for the initial layers was to ensure heat and material generation into the build plate. As the print progressed, the layer time was reduced due to the tapered design of the WAAM cross beam.

After six days of printing, the print was stopped. The printed build table of the MedUSA system. As the part curved its ends structure initially broke all the step clamps throughout the print. However, the end clamps were stronger than the step clamps and did not break. This led to the distortion of the part and steel

the final design was sliced and toolpaths were generated, deposition was performed.

5.2. Fabrication results and residual stress

The WAAM cross beam was printed at the ORNL Manufacturing Demonstration Facility (MDF). Due to the size, the print required multiple days to complete using 14 hr print days.

Before printing, the build plates were machined and placed on the build table as shown in Figure 9. The build plates were clamped down using steel step clamps. Because the print was upwards, the build table was also deformed as seen in Figure 10. The distortion of the edges was greater than 25 mm. Due to safety concerns, the print was discontinued at the state shown in Figure 10. The part was later removed from the build table.

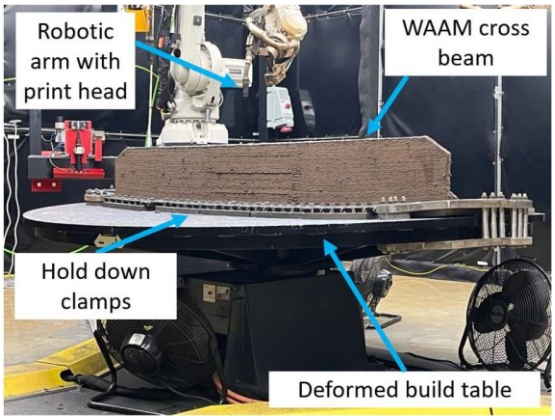

Fig. 10. Final state of the WAAM cross beam when the print was stopped. Deformation of the build table is observed.

The completed portion of the WAAM print had 245 completed layers and reached a height of 330 mm. The printed part was short by 271 mm. Approximately 406 kg of metal was deposited for the printed part. The remainder of the part was estimated to be approximately 122 kg. Using mass as an estimate, the part was 77% complete. Figure 11 identifies the stopping height and the model of the incomplete print.

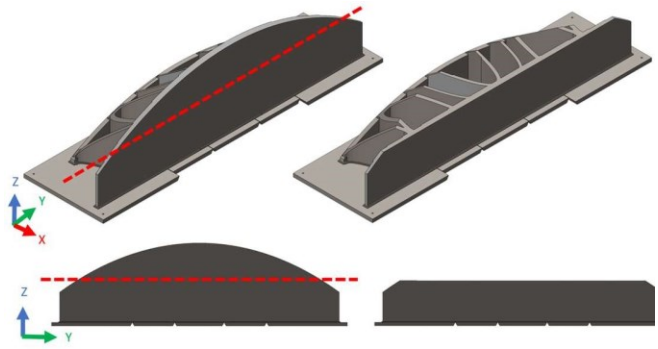

Fig. 11. (Left) Isometric and front views of the final designed cross beam and (right) incomplete print.

The print was stopped due to significant deformation of the part and build table. Once the print was stopped, the WAAM print was reviewed to understand the causes for the print deformation. The major factors included the design, build plates, fixturing, print strategy, and thermal behavior.

Two main concerns with the design were the aspect ratio of the part and the material choice. The cross beam's aspect ratio was about 1:3. This shape led to a long narrow print that could have increased distortion in the long axis. The weldment was constructed with A36 steel, and a comparable pintable material needed to be selected. The print material that had the most similar material properties to A36 was Lincoln Electric's LA100.

The build plates for this print were segmented to ideally allow relative motion. In addition, the interfaces between the plates were beveled. The beveled edges were to be used for post-print welding to join the individual plates. It is not clear what effect the segmentation and beveled edges had on the distortion. Because each plate was constrained by multiple step clamps, the overall effect was most likely not much different than a solid build plate.

6. Experimental results

6.1. FEA and measured natural frequencies and mode shapes of weldment

To compare the FEA simulation results with the impact testing data, mode shapes were extracted. Five modes with the largest amplitude from both the bottom and front face of the structure were selected for comparison. A large amplitude indicates lower dynamic stiffness and more importance for the machine tool's dynamic performance. Machine tool components are typically designed to be as stiff as possible. Considering the five least stiff modes on each face provides a baseline for the structure's dynamic behavior. In addition, the accuracy of the simulated mode shapes was verified using the experimental mode shapes.

Impact (tap) testing was used to measure the mode shapes. This testing was completed using a commercially-available measurement system [5]. A large modal hammer (PCB Piezotronics model 086D05), large magnetic single-axis accelerometer (PCB Piezotronics model 352C68), and data acquisition (DAQ) unit (Data Translation model DT9837B) were applied. The large modal hammer has a force sensor at the nylon tip. Due to the large weldment mass, an additional mass was added to the hammer head to increase the force input level and provide adequate excitation for good signal-to-noise ratio. The large, magnetic, single-axis accelerometer was chosen because it provided the required frequency range. Lastly, the DAQ was used to sample and record the time domain force and vibration signals. The commercial software was used to convert the time domain signals to the frequency domain and calculate the FRF for each measurement location and direction.

A grid coordinate system was used to select the individual points for impact testing, The row and column values for the bottom face are shown in Figure 12. For example, point (2,1) is associated with the point location that is in row 2 column 1.

The weldment was suspended using an overhead crane as seen in Figure 13. The weldment was supported upside down using rigging straps. This support simulated free-free boundary conditions.

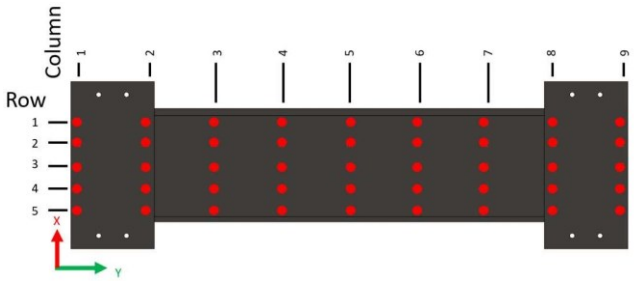

Fig. 12. Grid layout for the bottom face of the simplified weldment where each red point was a point of impact.

Fig. 13. Overhead crane lift of the weldment upside down for impact testing and approximate free-free boundary conditions.

To confirm that the weldment's FRF data was reliable, a reciprocity check was completed. For a first cross FRF measurement on the bottom face, the accelerometer was placed at point (1,1) while the impact was performed at point (1,9). The second cross FRF measurement on the bottom face was the opposite; the accelerometer was placed at point (1,9), and the impact was applied at point (1,1). The overlay of the real and imaginary plots for the two cross FRFs agreed, so it was demonstrated that reciprocity was achieved.

To find the five modes with the largest magnitudes from the bottom face measurements, the real and imaginary FRFs of the top row of points in Figure 12 were plotted together. By observing the peak values in the imaginary plot, the most flexible modes were chosen. The mode shape frequencies for the bottom face that were compared were {209, 373, 377, 413, and 545} Hz. The magnitudes for each impact location at the selected natural frequencies were identified using the peak imaginary part values. These magnitudes values were normalized to the direct FRF magnitude. The normalized magnitudes were then mapped to corresponding geometric coordinates to generate a surface that represented the mode shape.

The normalized points from peak picking for mode 1 (209 Hz) are displayed in Figure 14. The FEA mode shape is included for comparison.

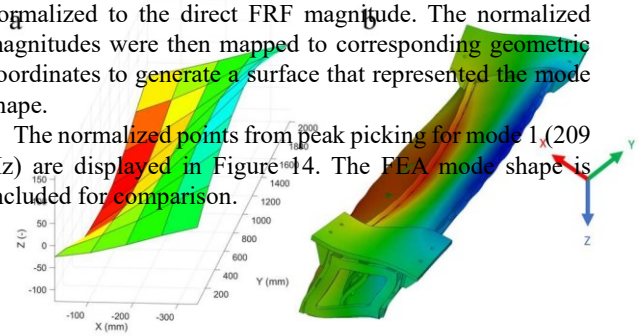

Fig. 14. (a) Measured mode shape (209 Hz) for the bottom face of the weldment; (b) corresponding FEA mode shape using the refined weldment model.

The five selected mode shapes showed good visual agreement. The measured and simulated natural frequencies are given in Table 1. The good agreement validates that the FEA model is sufficiently accurate to perform design studies prior to fabrication.

Table 1. Measured and predicted (FEA) natural frequencies for modes 1-5 for the bottom face of the weldment.

Mode	Measured [Hz]	Predicted [Hz]	Percent difference [%]
1	209	210	0.5
2	373	354	-5.4
3	377	373	-1.1
4	413	397	-4.0
5	545	520	-4.8

The modal damping ratio and stiffness values for the five mode shapes of the bottom face of the weldment were extracted from the measured FRFs. The results are shown in Table 2. The modal parameters were used to generate FRFs. The best fit FRF is superimposed on the measured direct FRF for point (1,1) in Figure 15.

Table 2. Modal damping ratio and stiffness values from the five measured modes of the weldment bottom face.

Mode	Natural frequency [Hz]	Damping ratio [-]	Stiffness [N/m]
1	209	0.006	2.43 × 10
2	373	0.004	2.40 × 10
3	377	0.006	4.50 × 10
4	413	0.007	2.75 × 10
5	545	0.005	5.30 × 10

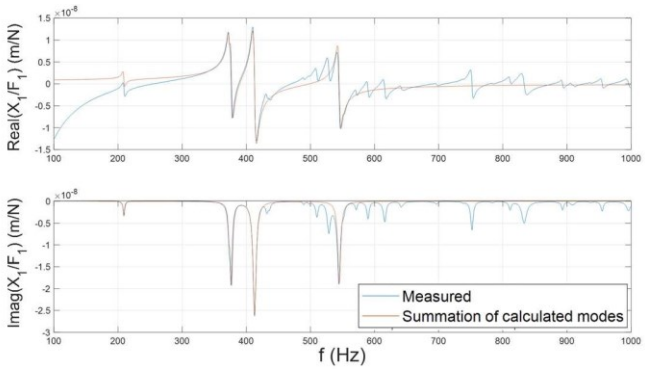

Fig. 15. Overlay of the measured and modal fit FRFs for the bottom face of the weldment.

The same procedure was followed for the front face of the weldment to find the respective mode shapes, natural frequencies, damping ratios, and stiffnesses. Mode 1 for the

front face occurred at 209 Hz. Figure 16 shows both the measured and predicted mode shape for the front surface. The measured and predicted natural frequencies for the five selected mode shapes of the front face are listed in Table 3. Table 4 provides the best fit modal damping ratio and stiffness values for the selected mode shapes.

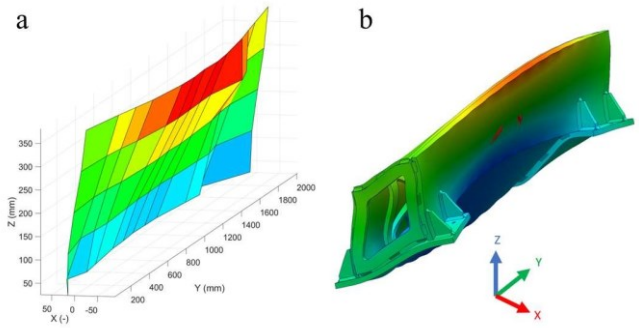

Fig. 16. (a) Measured mode shape (209 Hz) for the front face of the weldment; (b) corresponding FEA mode shape using the refined weldment model.

Table 3. Measured and predicted (FEA) natural frequencies for modes 1-5 for the front face of the weldment.

Mode	Measured [Hz]	Predicted [Hz]	Percent difference [%]
1	209	210	0.5
2	375	354	-5.9
3	529	505	-4.8
4	546	519	-5.2
5	833	800	-4.1

Table 4. Modal damping ratio and stiffness values from the five measured modes of the weldment front face.

Mode	Natural frequency [Hz]	Damping ratio [-]	Stiffness [N/m]
1	209	0.007	8.10 × 10
2	375	0.005	1.31 × 10
3	529	0.005	8.35 × 10
4	546	0.004	1.75 × 10
5	833	0.003	9.20 × 10

The modal parameters were used to generate FRFs. The best fit FRF is superimposed on the measured direct FRF for point (1,1) in Figure 17.

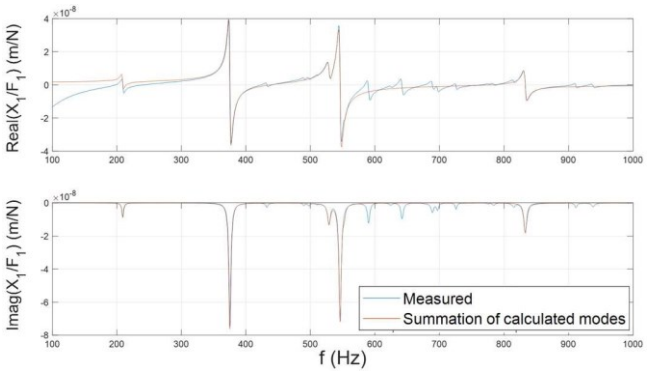

Fig. 17. Overlay of the measured and modal fit FRFs for the bottom face of the weldment.

6.2. Predicted and measured natural frequencies and mode shapes for mBAAM cross beam

Impact testing was used to measure the direct and cross FRFs of the printed WAAM cross beam. The final print, shown in Figure 10, was removed from the build table and impact tests were completed using the same equipment and methodology for the weldment. The WAAM cross beam's bottom face and front face were measured to identify the natural frequencies and mode shapes. A new FEA model with the appropriate geometry (Figure 11) was used to predict the natural frequencies and mode shapes.

The WAAM cross beam was also suspended using an overhead crane. As with the weldment, his support strategy approximated free-free boundary conditions. A grid of points for the bottom and front faces of the WAAM cross beam was defined to identify the mode shapes.

A roving hammer approach was applied where the accelerometer remained at the same location and the other locations were impacted to identify the cross FRFs.

The procedure followed for the weldment was repeated for the bottom face of the WAAM cross beam to find the natural frequencies, mode shapes, damping ratios, and stiffnesses. Mode 1 for the bottom face of the WAAM cross beam occurred at 184 Hz. Figure 18 shows both the measured and predicted mode shapes for this natural frequency. Table 5 provides a comparison of the measured and prediction natural frequencies. Table 6 gives the modal damping ratio and stiffness values for the selected mode shapes.

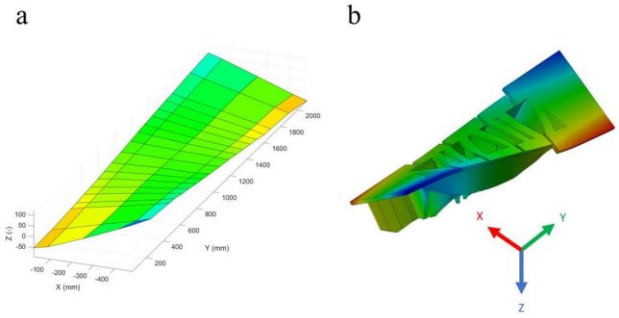

Fig. 18. (a) Measured mode shape (194 Hz) for the bottom face of the WAAM cross beam; (b) corresponding FEA mode shape.

Table 5. Measured and predicted (FEA) natural frequencies for modes 1-5 for the bottom face of the WAAM cross beam.

Mode	Measured [Hz]	Predicted [Hz]	Percent difference [%]
1	184	164	-12.2
2	233	245	4.9
3	291	293	0.7
4	377	469	19.6
5	687	704	2.4

Table 6. Modal damping ratio and stiffness values from the five measured modes of the WAAM cross beam bottom face.

Mode	Natural frequency [Hz]	Damping ratio [-]	Stiffness [N/m]
1	184	0.019	4.00 × 10
2	233	0.014	1.10 × 10
3	291	0.006	3.50 × 10
4	377	0.016	7.40 × 10
5	687	0.005	3.70 × 10

The modal parameters were used to generate FRFs. The best fit FRF is superimposed on the measured direct FRF for point (1,1) in Figure 19.

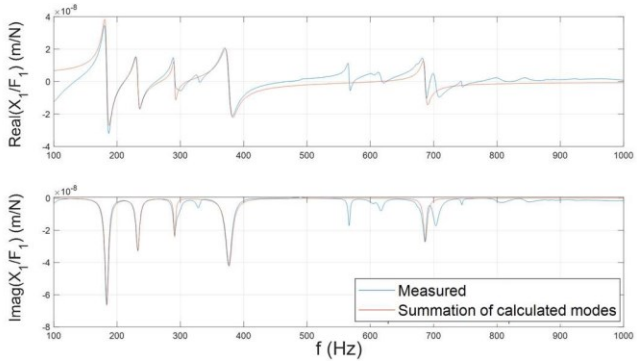

Fig. 19. Overlay of the measured and modal fit FRFs for the bottom face of the WAAM cross beam.

The procedure was repeated for the front face of the WAAM cross beam to find the respective natural frequencies, mode shapes, damping ratios, and stiffnesses. Mode 1 for the front face of the WAAM cross beam occurred at 483 Hz. Figure 20 shows measured and predicted mode shapes. The measured and predicted natural frequencies for the five selected mode shapes of the WAAM cross beam front face are listed in Table 7. Table 8 provides the modal damping ratio and stiffness values for the selected mode shapes.

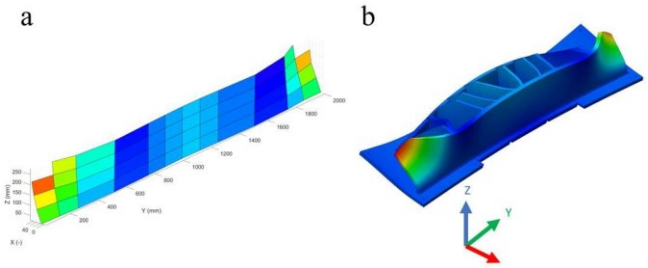

Fig. 20. (a) Measured mode shape (483 Hz) for the front face of the WAAM cross beam; (b) corresponding FEA mode shape.

Table 7. Measured and predicted (FEA) natural frequencies for modes 1-5 for the front face of the WAAM cross beam.

Mode	Measured [Hz]	Predicted [Hz]	Percent difference [%]
1	483	481	-0.4
2	486	483	-0.6
3	566	625	9.4
4	610	666	8.4
5	674	677	0.4

Table 8. Modal damping ratio and stiffness values from the five measured modes of the WAAM cross beam front face.

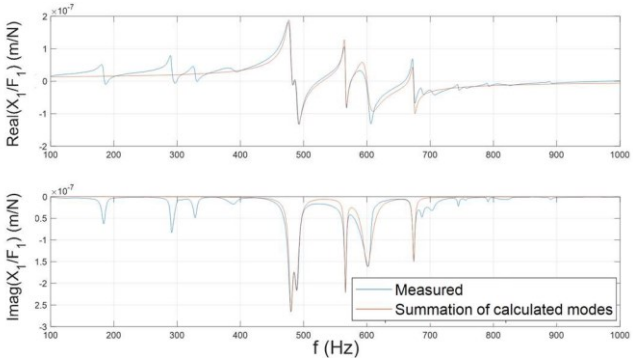

Mode	Natural frequency [Hz]	Damping ratio [-]	Stiffness [N/m]
1	483	0.019	1.82 × 10
2	486	0.014	4.40 × 10
3	566	0.006	7.90 × 10
4	610	0.016	2.09 × 10
5	674	0.005	1.15 × 10

Fig. 21. Overlay of the measured and modal fit FRFs for the front face of the WAAM cross beam.

The modal parameters were used to generate FRFs. The best fit FRF is superimposed on the measured direct FRF for point (1,1) in Figure 21.

The viscous damping ratio, ζ, is used to describe the behavior of damped systems [7]. Tables 9 and 10 present the measured damping ratios for the weldment and WAAM cross beam bottom and front faces. A higher damping ratio indicates

a higher vibrational decay rate, which is preferred to machining applications. The damping ratios from the bottom face of the weldment ranged from 0.004 to 0.007 with an average of 0.0056. The damping ratios from the bottom face of the WAAM cross beam ranged from 0.005 to 0.019 with an average of 0.012. This indicates that the WAAM cross beam's bottom face dissipates vibrational energy more efficiently than the weldment.

Table 9. Natural frequencies and damping ratios for the bottom face of the weldment and WAAM cross beam.

Cross beam	Mode number	Natural frequency [Hz]	Damping ratio [-]
Weldment	1	209	0.006
	2	373	0.004
	3	377	0.006
	4	413	0.007
	5	545	0.005
WAAM	1	184	0.019
	2	233	0.014
	3	291	0.006
	4	377	0.016
	5	687	0.005

Table 10. Natural frequencies and damping ratios for the front face of the weldment and WAAM cross beam.

Cross beam	Mode number	Natural frequency [Hz]	Damping ratio [-]
Weldment	1	209	0.007
	2	375	0.005
	3	529	0.005
	4	546	0.004
	5	833	0.003
WAAM	1	483	0.011
	2	486	0.007
	3	566	0.003
	4	610	0.015
	5	674	0.003

The damping ratios from the front face of the weldment ranged from 0.003 to 0.007 with an average of 0.004. The damping ratios from the bottom face for the WAAM cross beam ranged from 0.003 to 0.015 with an average of 0.008. As with the bottom face, the WAAM cross beam front face dissipates vibrational energy more efficiently than the weldment.

Several factors could have contributed to the higher damping ratios for the WAAM cross beam. One factor could be the WAAM design: the material concentration was higher near the interfaces that experience the largest force. Another factor could be the material itself, which was melted and solidified through the WAAM process.

Although the WAAM print was incomplete, impact testing of the printed structure provided insight into the WAAM structure's material and design properties. It was observed that the damping ratios were generally higher for the WAAM cross beam. It was also seen that the selected design was able to obtain similar natural frequencies, mode shapes, and stiffness values relative to the traditional box beam design for the weldment.

7. Discussion

Machine tool design requires that many variables are considered simultaneously. A method for assessing the redesign of a machine tool structure was presented. FEA was used to predict natural frequencies and mode shapes. The WAAM fabrication process, including path planning, was incorporated at the design stage.

A final design was selected to be manufactured with the MedUSA system. It had similar natural frequencies, mode shapes, and stiffness to the original weldment. The original weldment had a mass of 673 kg and the final designed WAAM cross beam had a mass value of 646 kg, which is 4% less mass than the weldment. Features of the final design were implemented to enable manufacturing by the WAAM process, including elimination of supports and overhangs, while also implementing features that reduced the mass.

The mode shapes for the weldment and the WAAM print were compared using FEA simulation and modal analysis through impact testing. With high fidelity FEA models, simulations of both structures were able to accurately predict the natural frequencies and mode shapes. Measurements of the physical structures validated the simulation accuracy.

7.1. Future work

The WAAM cross beam print revealed challenges. The part deformation caused the print to be discontinued. Distortion of the part could be assigned to various factors, including the method that the build plate was secured. The final printed part was measured using a GOM ATOS Q structured light scanner to compare the deformation of the WAAM print compared to the model shown in Figure 22. Future experiments will include modified clamping strategies [8] and updated print paths.

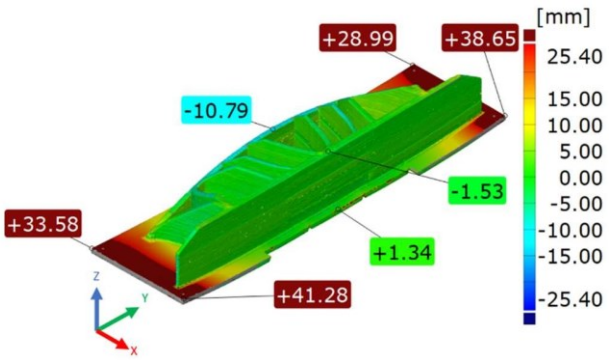

Fig. 22. Deviations of the final printed WAAM cross beam from the modeled and expected WAAM cross beam.

Although the WAAM cross beam was not fully printed, the implementation of the design, manufacturing, and testing processes provides a methodology for future mBAAM projects. For the 77% complete print, the modeling and measurement results showed promise and indicate that largescale WAAM prints are possible. Future work will focus on thermal distortion modeling and reduction.

8. Conclusions

This paper described the application of mBAAM to fabrication of a machine tool cross beam. A traditional box beam weldment was replaced by a new WAAM design printed by the MedUSA system at ORNL. The two designs were compared using natural frequencies and mode shapes obtained by impact testing and FEA. It was observed that the printed structure dynamics agreed with the numerical model predictions, which demonstrated that it is feasible to model an mBAAM part and predict its dynamic behavior prior to printing. Another notable outcome of this study is that the significant residual stress and distortion in the print indicate that knowledge gaps remain for widespread implementation of mBAAM.

Acknowledgements

This work was partially supported by the DOE Office of Energy Efficiency and Renewable Energy (EERE), Advanced Manufacturing Office (AMO), under contract DE-AC05-00OR22725. The US government retains and the publisher, by accepting the article for publication, acknowledges that the US government retains a nonexclusive, paid-up, irrevocable, worldwide license to publish or reproduce the published form of this manuscript, or allow others to do so, for US government purposes. DOE will provide public access to these results of federally sponsored research in accordance with the DOE Public Access Plan (http://energy.gov/downloads/doe-publicaccess-plan).

The authors knowledge support from the DoD Industrial Base Analysis and Sustainment Program (IBAS). The authors would also like to acknowledge support from the NSF Engineering Research Center for Hybrid Autonomous Manufacturing Moving from Evolution to Revolution (ERCHAMMER) under Award Number EEC-2133630. The wirearc technology used to create the cross beam was developed in collaboration with Lincoln Electric under a Cooperative Research and Development Agreement.

References

[1] West, J.L., Betters, E.D., Schmitz, T.L., Smith, S., Roschli, A., Nuttall, D., Lindahl, J. and Love, L., 2022. Rethinking production of machine tool bases: Polymer additive manufacturing and concrete. Manufacturing Letters, 31, pp.33-35.

[2] Arbogast, A., Nycz, A., Noakes, M. W., Wang, P., Masuo, C., Vaughan, J., Lind, R., Carter, W., Meyer, L., Vaughan, D., Walters, A., Patrick, S., Paul, J., & Flamm, J. (TBD). Strategies for a scalable multi-robot large scale wire arc additive manufacturing system. Additive Manufacturing Letters.

[3] A. A. Hassen, M. Noakes, P. Nandwana, S. Kim, V. Kunc, U. Vaidya, L. Love and A. Nycz, “Scaling up metal additive manufacturing process to fabricate molds for composite manufacturing,” vol. 32, p. 101093.

[4] Nikolić, D., 2019. Catenary arch of finite thickness as the optimal arch shape. Structural and Multidisciplinary Optimization, 60(5), pp.1957-1966. [5] T. L. Schmitz and K. S. Smith, “Modal analysis,” in Machining Dynamics: Frequency Response to Improved Productivity, Springer International Publishing, pp. 7-66.

[6] MetalMAX kit. [Online]. Available: http://mfglabs.weebly.com/store/p2/MetalMAX Kit.html

[7] T. L. Schmitz and K. S. Smith, “Single degree of freedom free vibration,” in Mechanical Vibrations: Modeling and Measurement, Springer US, pp. 25-81.

[8] West, J., Betters, E. and Schmitz, T., 2023. Limited-constraint WAAM fixture for hybrid manufacturing. Manufacturing Letters, 37, pp.66-69.